ACS OMEGA

Open Access

http://pubs.acs.org/journal/acsodf

Article

Geminal Dicationic Ionic Liquids (GDILs) and Their Adsorption on Graphene Nanoflakes

Mehdi Shakourian-Fard,* Hamid Reza Ghenaatian, and Ganesh Kamath

Cite This: *ACS Omega* 2024, 9, 7575−7587

Read Online

ACCESS | Metrics & More | Article Recommendations | Supporting Information

ABSTRACT: In this work, the configuration and stability of 15 geminal dicationic ionic liquids (GDILs) and their adsorption mechanism on the graphene nanoflake (GNF) are investigated using the density functional theory (DFT) method. We find that the interactions of dications ($[DAm]^+$, $[DIm]^+$, $[DImDm]^+$, $[DPy]^+$, and $[DPyrr]^+$)) are stabilized near the anions ($[BF_4]^-$, $[PF_6]^-$, and $[Tf_2N]^-$) in the most stable configurations of GDILs through electrostatic interactions, van der Waals (vdW) interactions, and hydrogen bonding (H-bonding). Our calculations show that the adsorption of the GDILs on the GNF is consistent with the charge transfer and occurs via X···π (X = N, O, F), C−H···π, and π···π noncovalent interactions, leading to a decrease in the strength of the intermolecular interactions between the dications and anions in the GDILs. The thermochemistry calculations reveal that the formation of GDIL@GNF complexes is an exothermic and favorable reaction. The adsorption energy (E_{ads}) calculations show that the highest E_{ads} values for the interaction of GDILs containing $[BF_4]^-$, $[PF_6]^-$, and $[Tf_2N]^-$ anions with the GNF are observed for the [DPy][BF_4]@GNF (−23.56 kcal/mol), [DPy][PF_6]@GNF (−29.29 kcal/mol), and [DPyrr][Tf_2N]@GNF (−24.74 kcal/mol) complexes, respectively. Our results show that the adsorption of the GDILs on the GNF leads to the decrease of the chemical potential (μ), chemical hardness (η), and HOMO−LUMO energy gap (E_g) values and an increase in the electrophilicity index (ω) value of the GNF. In addition, the effect of GDIL adsorption on the UV−vis absorption spectrum was studied at the TD-M06-2X/cc-pVDZ level of theory. We find that the adsorption of GDILs results in minimal change in the shape of the main absorption peak (at λ = 363 nm) in the GNF spectrum and only shifts it to higher wavelengths. On the other hand, a new peak appears in the GNF spectrum upon adsorption of [DPy][Y] (Y = $[BF_4]^-$, $[PF_6]^-$, and $[Tf_2N]^-$) due to the relatively strong π···π interactions between the $[DPy]^+$ dication and GNF. Finally, the transition density matrix (TDM) heat maps show that electron transfers related to the excitation states in the GDIL@GNF complexes occur mainly through π(C═C) → π*(C═C) transitions in the GNF and the transitions from $[DPy]^+$ dication to the GNF.

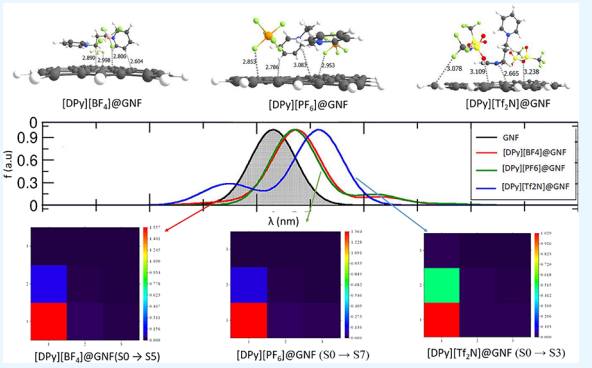

1. INTRODUCTION

Graphene is the world's thinnest two-dimensional carbon material with a honeycomb-like pattern.[1−4] It is one of the most exciting materials, and many aspects of its potential applications are explored in diverse fields such as electronics, smart coatings, sensing, energy management systems, photonics, and biomedicine with drug delivery.[5−7] Moreover, since graphene was first isolated in 2004, it has shown outstanding physical properties that make it a hot spot in research. For instance, the unique energy band structure, ultrathin body, and high electron mobility of graphene contribute to its appeal and make it the material of the future.[8] Graphene is the mother of all graphitic materials including 1D carbon nanotubes, 3D graphite, and fullerenes. Although these carbonaceous materials have the same root, they are significantly different in electronic, mechanical, optical, and thermal characteristics because of their diverse structures.[9] Nowadays, research on graphene and its derivatives has experienced a sharp exponential growth due to the infinite possibilities to modify.[10−13] However, the development of technologies to produce large amounts of graphene is important for scientific research and industry. Over the past few years, liquid-phase exfoliation of graphite has been achieved using numerous techniques and solvents to achieve large scalable graphene. However, these techniques have several weaknesses related to controllability performance, accessibility, and cost. Therefore, there is a need to develop a simple and low-cost method for preparing high-quality graphene without the need for common volatile and toxic organic solvents.[14] Ionic liquids (ILs) as a new class of solvents with a low melting point, negligible vapor

Received: September 1, 2023
Revised: January 10, 2024
Accepted: January 23, 2024
Published: February 6, 2024

Scheme 1. Schematic Diagram Showing the Structures of the GNF Model and the Constituents of GDILs Studied in This Work

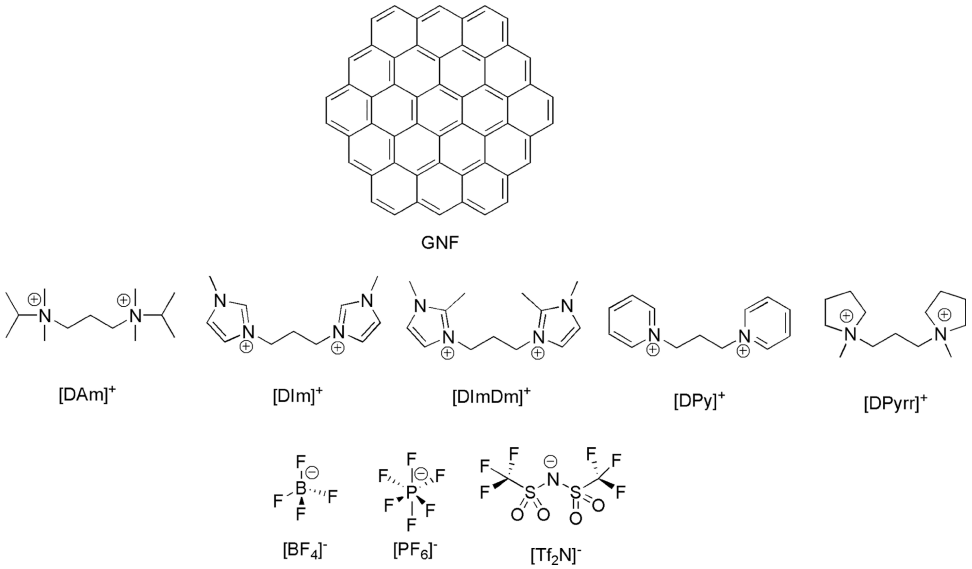

pressure, solvating power, high selectivity, inertness, ease of reuse, and good chemical and thermal stability have been used in liquid-phase exfoliation of graphite and improved the electronic structure of graphene surfaces.[15−17]

Several works have represented the efficient dispersion of graphene[18,19] and its derivatives using ILs, e.g., carbon nanotubes[20] and fullerene.[21,22] The interactions between ions and π electrons in graphene (ion−π interactions) would be responsible for the solvation of graphitic planes.[23] As per the literature data, physicochemical properties of ILs can be adjusted by changing the structure of their cations and anions to disperse graphene flakes efficiently.[24,25] Moreover, green chemistry is devoted to optimizing synthetic procedures that minimize environmental impacts. Therefore, for introducing a more efficient and environmentally sustainable IL with a structured design framework, chemists and molecular designers merge a collection of skills. For all these reasons, attention has focused on a new subclass of ILs named dicationic ionic liquids (DILs), which are less toxic than their monocationic counterparts.[26] In contrast to ILs with a single cation, DILs have higher densities, viscosities, and glass transition temperatures. Various DILs have been synthesized in the literature. For example, Cecchini et al.[27] synthesized mono-, di-, or tricationic poly(ethylene glycol)-based ionic liquids (ILPEGs) and determined their viscosity or thermal stability. In another study,[28] they reviewed the strategies for the synthesis of poly(ethylene glycol)-based DILs and highlighted their physicochemical properties and their applications. Kaczmarek et al.[29] synthesized new DILs based on quaternary bis-(ammonium) dications and determined their properties containing density, solubility, viscosity, and refractive index. Roohi et al.[30] investigated the physical and chemical properties of dicationic imidazolium-based ILs with an ethylene π-spacer using density functional theory (DFT) calculations. They found that the structural and electronic properties of these DILs can be tuned for particular applications by changing the anion type. Moosavi et al.[31] studied the properties of the bulk liquid phase of two imidazolium-based DILs ($[C_n(mim)_2][NTf_2]_2$ (n = 3 and 5)) using molecular dynamics (MD) simulations and DFT calculations. In another investigation, Alavi and Yeganegi[32] investigated the intermolecular interactions in the ion pairs composed of bis-imidazolium dication and two halogen-free boron-based anions including bis-(manolato)borate $[BMLB]^-$ and bis(oxalato)borate $[BOB]^-$ using DFT calculations. Their results indicated that the hydrogen bonding (H-bonding) and electrostatic interactions have an effective role in the stabilization of the ion pairs. They also studied the structures and dynamics of nine dicationic ILs, ($[C_n(mim)_2][X]_2$ (n = 3, 6, 9 and X = Br^-, BF_4^-, and PF_6^-) by MD simulations and determined their density values and microscopic structures.[33]

Recently, Matsumoto et al. used microwave-assisted exfoliation of graphite into single-layer graphene using oligomeric ionic liquids of IL_2PF_6 and IL_4PF_6 as fluid media.[34] Li et al.[35] studied the structure and capacitance of the electrical double layers (EDLs) in imidazolium-based DILs concerning monocationic ionic liquids close to carbon electrodes containing graphene sheets. They observed that the imidazolium cations paired with anions are strongly adsorbed near the electrode surface. However, there is a long way to go to fully understand the chemical functionality of DILs as a suitable reaction medium for stabilizing graphene sheets.[36] However, good information on the nature and strength of the interaction of DIL components with graphene can be evaluated using computational investigations. These methods are effective techniques to understand the behavior and structure of materials at the interfaces. Moreover, they are affordable, accurate, and fast screening tools and are necessary to provide a piece of good information on the nature and strength of interactions between cationic and anionic moieties of DILs and graphene.[37] However, experimental and theoretical studies have not yet grown enough, and there are very few studies on the interaction of DILs and graphene sheets.

In this study, the configuration and stability of 15 types of geminal dicationic ionic liquids (GDILs) and their adsorption mechanism on the graphene nanoflake (GNF) are investigated at the M06-2X/cc-pVDZ level of theory. The thermodynamic properties, nature and strength of interactions, reactivity parameters, UV−vis spectra, and transition density matrix

https://doi.org/10.1021/acsomega.3c06581
ACS Omega 2024, 9, 7575−7587

(TDM) heat maps of the GDILs and their complexes with GNF are also considered.

2. COMPUTATIONAL DETAILS

In recent years, the density functional theory (DFT) methods have been widely used for providing the structural and electronic properties of germinal dicationic ionic liquids (GDILs).[30,32,38] In this study, the adsorption of GDILs based on diammonium $[DAm]^+$, di-imidazolium $[DIm]^+$, di-imidazolium-dimethyl $[DImDm]^+$, dipyridinium $[DPy]^+$, and dipyrrolydinium $[DPyrr]^+$ cations combined with common $[BF_4]^-$, $[PF_6]^-$, and $[Tf_2N]^-$ anions on the pristine graphene nanoflake (GNF) (Scheme 1) was investigated. The graphene nanoflake is modeled by one central C_6-ring surrounded by two layers of adjacent C_6-rings (circumcoronene model; $C_{54}H_{18}$). In the GNF model, the hydrogen atoms saturate the dangling bonds at the terminal carbon atoms. The GNF model has already been used for investigating the interaction of ILs with graphene in the literature.[39−42]

The M06-2X functional in conjunction with Dunning's correlation-consistent, polarized valence, double-ζ (cc-pVDZ) basis set was used in this study to optimize the initial geometries of the GDILs and their complexes with GNF. Furthermore, the effects of dispersion correction on the adsorption strength of GDILs on the GNF model were explored by using Grimme's D3 dispersion correction.[43−45] The M06-2X density functional is useful for main group thermochemistry, kinetics, and noncovalent interactions.[46] This functional is reliable for predicting noncovalent interactions due to using 54% HF exchange energy, which is not well described by the non-long-range corrected DFT methods. Furthermore, the M06-2X functional has been widely used in the literature for investigating the interaction of ILs with different surfaces such as graphene,[39,47] defective graphene,[40] nitrogen-doped graphene,[48] fluorographene,[49] hexagonal boron nitride,[50−52] defective hexagonal boron nitride,[52,53] and boron nitride nanotubes.[54]

The optimization of the initial geometries was performed with no symmetry restriction. The calculated vibrational frequencies for the optimized geometries were checked to make sure that the global minima are real. All the geometry optimizations and electronic structure calculations were done using the Gaussian 09 package.[55]

To calculate the binding energy in the GDILs (E_b), the sum of the energies of isolated components of GDILs ($E_{(dication)}$ and $E_{(anion)}$) was subtracted from the total energy of the GDILs ($E_{(GDIL)}$) according to eq 1:

$$E_b = E_{(GDIL)} - (E_{(dication)} + 2E_{(anion)}) + BSSE \quad (1)$$

In addition, the adsorption energies of GDILs on the GNF (E_{ads}) were calculated using eq 2:

$$E_{ads} = E_{(GDIL@GNF)} - (E_{(GDIL)} + E_{(GNF)}) + BSSE \quad (2)$$

In this equation, $E_{(GDIL@GNF)}$, $E_{(GDIL)}$, and $E_{(GNF)}$ terms correspond to the total energy of the GDIL@GNF complexes, GDILs, and GNF, respectively.

The E_b and E_{ads} values in eqs 1 and 2 were corrected by the basis set superposition error (BSSE) calculated according to the counterpoise method.[56] The distribution of charge density in the GNF, GDILs, and their constituents was observed by calculating the electrostatic potential (ESP) maps.[57,58] The ChelpG charge calculations[59] were done at the M06-2X/cc-pVDZ level of theory to calculate the charge transfer amount in the GDILs and GDIL@GNF complexes.

The thermodynamic properties such as change in enthalpy (ΔH) and change in Gibbs free energy (ΔG) for the formation of GDILs and GDIL@GNF complexes were calculated at 298.15 K using eqs 3 and 4:

$$\Delta Y_{(GDIL)} = Y_{(GDIL)} - (Y_{(dication)} + 2Y_{(anion)}) \quad (3)$$

$$\Delta Y_{(GDIL@GNF)} = Y_{(GDIL@GNF)} - (Y_{(GDIL)} + Y_{(GNF)}) \quad (4)$$

$$Y = H(\text{enthalpy}) \text{or } G(\text{free energy})$$

where $Y_{(dication)}$, $Y_{(anion)}$, $Y_{(GNF)}$, $Y_{(GDIL)}$, and $Y_{(GDIL@GNF)}$ terms are the H or G of the dications, anions, GNF, GDILs, and GDIL@GNF complexes, respectively. Also, the change in entropy (ΔS) for the GDILs and GDIL@GNF complexes was calculated at 298.15 K according to eq 5:

$$\Delta S_{(GDIL/GDIL@GNF)} = \frac{(\Delta H_{(GDIL/GDIL@GNF)} - \Delta G_{(GDIL/GDIL@GNF)})}{298.15} \quad (5)$$

The reactivity parameters including the highest occupied molecular orbital (HOMO), the lowest unoccupied molecular orbital (LUMO), HOMO−LUMO energy gap ($E_g = E_{LUMO} - E_{HOMO}$), chemical hardness ($\eta = (E_{LUMO} - E_{HOMO})/2$), chemical potential ($\mu = (E_{HOMO} + E_{LUMO})/2$), and electrophilicity index ($\omega = \mu^2/2\eta$)[60−63] were calculated for the GNF and GDIL@GNF complexes.

The quantum theory of atoms in molecules (QTAIM) analysis[64] was performed for the calculation of electron density and its derivatives using the AIM2000 program[65] at the M06-2X/cc-pVDZ level of theory. The role of noncovalent interactions in the formation of GDILs and GDIL@GNF complexes was determined by plotting the noncovalent interactions (NCIs) calculated by the Multiwfn-3.2 program[66] and visualized by the VMD program.[67] The UV−vis absorption spectra of GNF and GDIL@GNF complexes were calculated using the TD-M06-2X/cc-pVDZ method. Ten excited states were considered, and the absorption spectra were generated by a normalized Gaussian line shape function with a full width at half-maximum (fwhm) of 14 nm. Finally, the transition density matrix (TDM) heat maps of GDIL@GNF complexes were obtained using the Multiwfn-3.2 program to understand how the charge transfer occurs through the excited states in the GDIL@GNF complexes.

3. RESULTS AND DISCUSSION

3.1. Configuration and Stability of Geminal Dicationic Ionic Liquids (GDILs). To determine the most stable configuration of geminal dicationic ionic liquids (GDILs), the electrostatic potential (ESP) maps of the optimized dications ($[DAm]^+$, $[DIm]^+$, $[DImDm]^+$, $[DPy]^+$, $[DPyrr]^+$) and anions ($[BF_4]^-$, $[PF_6]^-$, $[Tf_2N]^-$) were calculated at an isovalue electron density (0.0004 au) and presented in Figure S1 (Supporting Information). In these maps, the intensity of electrostatic potential energies is shown by a contour plot. The regions with the highest positive charge density (favorable for the interaction of nucleophiles) are shown in blue color, whereas the regions with the highest negative charge density (favorable for the interaction of electrophiles) are presented in red color. In the intermolecular interactions, the regions in blue color always tend to interact with the regions in red color and vice versa. As seen in Figure S1, the entire molecular

https://doi.org/10.1021/acsomega.3c06581
ACS Omega 2024, 9, 7575−7587

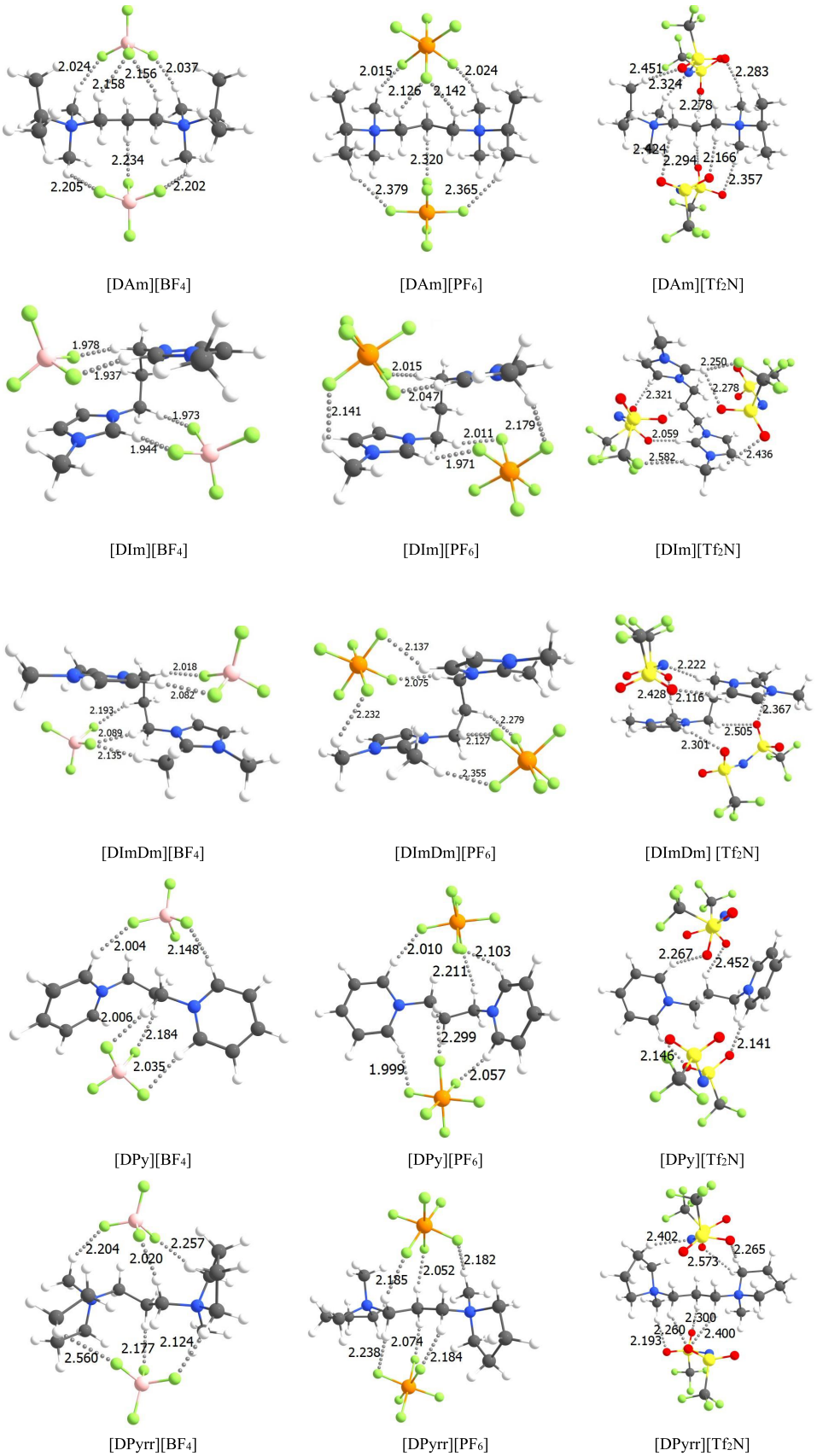

Figure 1. The most stable optimized configurations of GDILs are calculated at the M06-2X/cc-pVDZ level of theory.

regions of anions and cations show a negative and positive charge density, respectively. A negative charge density (red color) in the $[BF_4]^-$, $[PF_6]^-$, and $[Tf_2N]^-$ anions is seen over the nitrogen (N), oxygen (O), and fluorine (F) atoms. On the

https://doi.org/10.1021/acsomega.3c06581
ACS Omega 2024, 9, 7575−7587

Table 1. Binding Energy (E_b in kcal/mol), Enthalpy Change (ΔH_{GDIL} in kcal/mol), Entropy Change (ΔS_{GDIL} in cal/mol·K), Gibbs Free Energy Change (ΔG_{GDIL} in kcal/mol), and Charge Transfer ($\Delta Q_{(anion)\rightarrow(cation)}$ in e) Values for the GDILs Calculated at the M06-2X/cc-pVDZ Level of Theory

structure	E_b	ΔH_{GDIL}	ΔS_{GDIL}	ΔG_{GDIL}	$\Delta Q_{(anion)\rightarrow(cation)}$
[DAm][BF_4]	−256.23	−276.38	−92.49	−248.81	−0.3791
[DAm][Tf_2N]	−250.91	−265.19	−94.91	−236.89	−0.2898
[DAm][PF_6]	−243.93	−263.74	−85.88	−238.13	−0.3616
[DIm][BF_4]	−253.95	−273.48	−98.33	−244.16	−0.4160
[DIm][Tf_2N]	−246.09	−261.62	−104.29	−230.53	−0.3097
[DIm][PF_6]	−241.69	−260.51	−89.168	−233.92	−0.3262
[DImDm][BF_4]	−247.61	−268.20	−101.52	−237.93	−0.4042
[DImDm] [Tf_2N]	−236.26	−257.68	−103.10	−226.94	−0.1636
[DImDm][PF_6]	−234.88	−255.05	−88.129	−228.77	−0.3309
[DPy][BF_4]	−259.62	−276.94	−87.71	−250.79	−0.4247
[DPy][Tf_2N]	−249.40	−261.95	−91.96	−234.53	−0.3983
[DPy][PF_6]	−245.10	−261.14	−74.50	−238.93	−0.4009
[DPyrr][BF_4]	−258.54	−278.12	−88.45	−251.75	−0.4434
[DPyrr][Tf_2N]	−249.69	−266.67	−101.22	−236.49	−0.3151
[DPyrr][PF_6]	−247.59	−264.43	−71.22	−243.19	−0.3956

other hand, a positive charge density in the $[DAm]^+$, $[DIm]^+$, $[DImDm]^+$, $[DPy]^+$, and $[DPyrr]^+$ cations is seen over the hydrogen (H) atoms at the imidazolium, methylimidazolium, pyridinium, and pyrrolidinium rings as well as methylene, methyl, and isopropyl groups.

To find the most stable configurations of GDILs, all possible orientations for the interaction of anions with the dications were considered by putting the anions around the dications at different spatial positions. These structures were then optimized at the M06-2X/cc-pVDZ level of theory and arranged from the lowest to the highest energy. Finally, the configurations with the most negative energy (the lowest energy) were determined for each GDIL and shown in Figure 1.

One can easily see from Figure 1 that the anions can be stabilized near the dications through electrostatic interactions, van der Waals (vdW) interactions, and hydrogen bonds. The bond lengths related to the hydrogen bond in the GDILs, including C−H···F, C−H···O═S, and C−H···N, are shown in Figure 1. The noncovalent interactions in the GDILs can be evaluated by the reduced density gradient (RDG) analysis. To characterize the strength and nature of these interactions, the sign of the second Hessian eigenvalue (sign (λ_2) multiplied by the electron density ($\rho(r)$), sign (λ_2)$\rho(r)$, is plotted onto the RDG isosurface, known as two-dimensional (2D) scatter plots.[68] In these plots, the sign (λ_2) determines the nature of noncovalent interaction, whereas the $\rho(r)$ value determines the strength of noncovalent interaction. A negative sign for the λ_2 value shows attractive interactions such as H-bonding, $\pi-\pi$ interactions, and electrostatic interactions, whereas a positive value shows repulsive interactions such as steric effects. The values near zero show very weak interactions and vdW interactions. In the RDG isosurfaces, electrostatic interactions are shown in blue color, H-bonding and vdW interactions in green color, and repulsive interactions in red color. Figure S2 shows the calculated RDG and 2D scatter plots for the GDILs to differentiate the attractive interactions from repulsive interactions. As seen from Figure S2, the noncovalent interaction regions between the dications and anions are mapped by green color. The green color reveals that the nature of interaction in the GDILs is weak vdW. These green regions are characterized by the cooperative C−H···F, C−H···O═S, C−H···N, and π···X (X = N, O, F) interactions. In addition, the repulsive interactions (red regions) are mostly observed in the imidazolium, methylimidazolium, pyridinium, and pyrrolidinium rings of the dications.

As seen from Figure 1, in the [DAm] [X] ([X] = $[BF_4]^-$, $[PF_6]^-$, and $[Tf_2N]^-$) ILs, the $[DAm]^+$ cation has no aromatic ring in its structure, and the anions lie close to the positive nitrogen atoms through forming the H-bonding interactions with the methylene, methyl, and isopropyl groups. About [DIm][X] ([X] = $[BF_4]^-$, $[PF_6]^-$, and $[Tf_2N]^-$) ILs, the anions have an important H-binding interaction with the C−H bond between nitrogen atoms in the imidazolium aromatic rings through C−H···O═S, and C−H···F interactions. These interactions have the shortest bond lengths in the ILs, and their bond lengths follow the order [DIm][Tf_2N] (2.059 Å, 2.278 Å)> [DIm][PF_6] (1.971 Å, 2.047 Å)> [DIm][BF_4] (1.937 Å, 1.944 Å). Previous studies have shown that these interactions are the most characteristic in the ILs based on imidazolium and di-imidazolium cations.[30,42] By replacing the hydrogen atom in the C−H bonds between two nitrogen atoms in the imidazolium aromatic rings with methyl ($-CH_3$) groups, these H-bonding interactions disappear; see the configurations of [DImDm][X] ([X] = $[BF_4]^-$, $[PF_6]^-$, and $[Tf_2N]^-$) ILs. Therefore, the anions move up and down methylimidazolium rings because of the steric hindrance caused by methyl groups in front of the imidazolium rings and are stabilized through the H-bonding and especially π···X (X = N, O, F) interactions. In the case of [DPy][X] and [DPyrr][X] ([X] = $[BF_4]^-$, $[PF_6]^-$, and $[Tf_2N]^-$) ILs, the anions lie close to the positive nitrogen atoms through forming the H-bonding interactions with the C−H bonds of pyridinium and pyrrolidinium rings as well as methylene and methyl groups. Interestingly, the anions do not tend to be placed on top of the pyridinium aromatic rings and nonaromatic pyrrolidinium rings.

The physical and chemical properties of ionic liquids are influenced by intermolecular interactions. The intermolecular interactions and thus the binding energy values in the ILs can be controlled by changing the type of anions and cations and their possible configurations for interaction.[69] The binding energy (E_b), change in entropy (ΔS_{GDIL}), change in enthalpy (ΔH_{GDIL}), and change in Gibbs free energy (ΔG_{GDIL}) for the formation of GDILs were calculated based on eqs 3 and 5 and

https://doi.org/10.1021/acsomega.3c06581
ACS Omega 2024, 9, 7575−7587

listed in Table 1. Table 1 shows that the E_b values for the GDILs are in the range of −234.88 to −259.62 kcal/mol. A comparison between these values and those calculated for Monocationic ILs at the same level of theory shows that the intermolecular interactions in the GDILs are stronger than monocationic ILs.[39,40,50] This is due to the increase in the number of anions and positive nitrogen atoms in the GDILs concerning monocationic ILs, enhancing the noncovalent interactions and E_b values in the GDILs. The results summarized in Table 1 show that the highest E_b values for the interaction of $[BF_4]^-$, $[PF_6]^-$, and $[Tf_2N]^-$ anions with the dications are observed for the [DPy][BF_4] (−259.62 kcal/mol), [DPyrr][PF_6] (−247.59 kcal/mol), and [DAm][Tf_2N] (−250.91 kcal/mol) GDILs, respectively. Based on the calculated E_b values, the stability of GDILs shows the order [X][BF_4] > [X][Tf_2N] > [X][PF_6] (X = $[DAm]^+$, $[DIm]^+$, $[DImDm]^+$, $[DPy]^+$, and $[DPyrr]^+$). A look at the RDG plots of the GDILs in Figure S2 confirms this result and shows that the degree of noncovalent interactions (the green regions) in the [X][BF_4] GDILs is more than [X][Tf_2N] and [X][PF_6] GDILs. Therefore, it can be concluded that the noncovalent interactions have a significant role to determine the stability of GDILs. Furthermore, according to the ESP map of $[Tf_2N]^-$ anion, it seems that the presence of powerful electron-withdrawing $-CF_3$ groups in the $[Tf_2N]^-$ anion decreases the electron density value on the oxygen atoms in the − S═O groups, decreasing the interaction strength of $[Tf_2N]^-$ anion and putting its interaction strength between $[BF_4]^-$ and $[PF_6]^-$ anions. It is worth pointing out that the observed order for the interaction of $[BF_4]^-$, $[PF_6]^-$, and $[Tf_2N]^-$ anions is in accordance with the results observed for the interaction of these anions with the imidazolium-based dicationic ionic liquids containing an ethylene π-spacer reported by Roohi et al.[30]

The ΔS_{GDIL}, ΔH_{GDIL}, and ΔG_{GDIL} values for the formation of GDILs were calculated to gain more details about the intermolecular interactions. Negative ΔH_{GDIL} values show that the intermolecular interactions for the formation of GDILs are favorable and the reaction is exothermic. As shown in Table 1, the highest ΔH_{GDIL} values for the interaction of $[BF_4]^-$, $[PF_6]^-$, and $[Tf_2N]^-$ anions with the dications are seen for the [DPyrr][BF_4] (−278.12 kcal/mol), [DAm][PF_6] (−263.74 kcal/mol), and [DPyrr][Tf_2N] (−266.67 kcal/mol) GDILs, respectively. In addition, the ΔH_{GDIL} values for the formation of GDILs follow the same order observed for the E_b values, i.e., [X][BF_4] > [X][Tf_2N] > [X][PF_6] (X = $[DAm]^+$, $[DIm]^+$, $[DImDm]^+$, $[DPy]^+$, and $[DPyrr]^+$). It should be mentioned that the formation of GDILs through intermolecular interactions decreases the degrees of freedom of the anions and dications, leading to the negative ΔS_{GDIL} values. Therefore, the calculation of ΔG_{GDIL} values, which are related to the ΔH_{GDIL} and ΔS_{GDIL} values, gives a more accurate measure of the behavior of anions and dications in the formation of GDILs. As shown in Table 1, all the calculated ΔG_{GDIL} values for the GDILs are negative and show that the formation of GDILs proceeds favorably through intermolecular interactions.

From Table 1, it is observed that the highest ΔG_{GDIL} values for the interaction of $[BF_4]^-$, $[PF_6]^-$, and $[Tf_2N]^-$ anions with the dications are seen for the [DPyrr][BF_4] (−251.75 kcal/mol), [DPyrr][PF_6] (−243.19 kcal/mol), and [DAm][Tf_2N] (−236.89 kcal/mol) ≈ [DPyrr][Tf_2N] (−236.49 kcal/mol) GDILs, respectively. Additionally, the ΔG_{GDIL} values for the GDILs show a different order than that observed for the E_b and ΔH values, following the order [X][BF_4] > [X][PF_6] > [X][Tf_2N] (X = $[DAm]^+$, $[DIm]^+$, $[DImDm]^+$, $[DPy]^+$, and $[DPyrr]^+$) and indicating the role and significance of the ΔS_{GDIL} term in the formation and stability of GDILs.

The ChelpG charge analysis was performed to quantify the amount of charge transfer in the GDILs. The amounts of charge transfer in the GDILs ($\Delta Q_{(anion)\rightarrow(cation)}$) were calculated through the charge difference of anions before and after interaction with the dications and are summarized in Table 1. As shown in Table 1, the highest charge transfer is seen in the [DPyrr][BF_4] (−0.4434e), and the lowest charge transfer is observed in the [DImDm][Tf_2N] (−0.1636e). Our results show that the amount of $\Delta Q_{(anion)\rightarrow(cation)}$ in the GDILs decreases from $[BF_4]^-$ to $[Tf_2N]^-$ and follows the order [X][BF_4] > [X][PF_6] > [X][Tf_2N]. This feature can be observed because of the increased distribution of negative charge over the anions with increasing anion size from $[BF_4]^-$ to $[Tf_2N]^-$.

3.2. Adsorption of GDILs on the GNF. To find the most stable optimized configurations of GDIL@GNF complexes, the ESP maps of GNF and GDILs were calculated and are shown in Figure S1. As seen from the ESP map of GNF, the center of GNF shows a negative electrostatic potential, which is suitable for interaction with the regions of GDILs with positive electrostatic potential. The hydrogen atoms used for saturation of the dangling bonds at the terminal carbon atoms show a positive electrostatic potential. For the GDILs, the regions with negative electrostatic potential are seen over the N, O, and F atoms of the $[BF_4]^-$, $[PF_6]^-$, and $[Tf_2N]^-$ anions, whereas the regions with positive electrostatic potential are observed over the N atoms, C−H bonds, and positive aromatic and nonaromatic rings in the dications. To find the most stable optimized configurations of GDIL@GNF complexes, all possible orientations for the interaction of GDILs with GNF were considered by putting the GDILs in the center of GNF at a distance of 2.7 Å through the regions with positive and negative electrostatic potentials. Then, these structures were optimized at the M06-2X/cc-pVDZ level of theory and sorted based on their energy from the lowest to the highest energy. Finally, the configurations with the lowest energy (the most negative energy) were determined for each GDIL@GNF complex and are shown in Figure 2.

The nearest distances between the GDILs and GNF are shown in Figure 2. A comparison between them shows that the nearest distance of dications from the GNF is shorter than that of anions, indicating that the dications have stronger interaction with the GNF than the anions. This is due to the presence of positive electrostatic potential on the dications in the GDILs, unlike the negative electrostatic potential on the anions, which promotes the intermolecular interactions with the GNF containing negative electrostatic potential.

Furthermore, the sum of electron density ($\sum\rho(r)$) values at the bond critical points (BCPs) formed between the dications and anions in the GDILs and the GDILs adsorbed on the GNF (Figures S3 and S4) was calculated using the AIM2000 program[22] at the M06-2X/cc-pVDZ level of theory. The positive sign of the difference between $\sum\rho(r)$ values ($\Delta\sum\rho(r)$), listed in Table 2, shows that the strength of the intermolecular interactions between the dications and anions in the GDILs decreases upon adsorption on the GNF.

As seen from Figure S5, the green regions between the $[BF_4]^-$, $[PF_6]^-$, and $[Tf_2N]^-$ anions and GNF show that the anions are adsorbed on the surface through X···π (X = N, O,

https://doi.org/10.1021/acsomega.3c06581
ACS Omega 2024, 9, 7575−7587

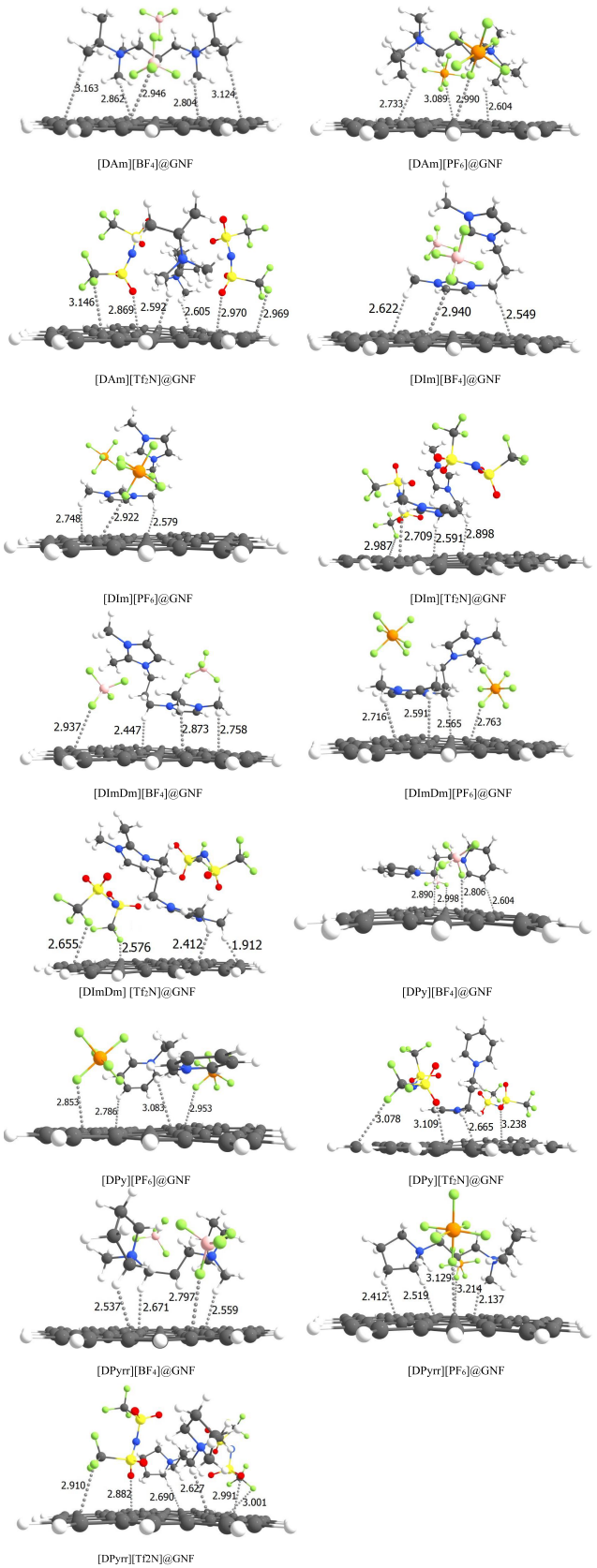

Figure 2. The most stable optimized configurations of GDIL@GNF complexes are calculated at the M06-2X/cc-pVDZ level of theory. All the nearest distances between the GDILs and GNF are in angstrom (Å).

F) vdW interactions. The adsorption behavior of dications containing aromatic rings ($[DIm]^+$, $[DImDm]^+$, and $[DPy]^+$) is different from other dications. As seen from Figure 2, one of the aromatic rings in the $[X][BF_4]$, $[X][PF_6]$, and $[X][Tf_2N]$ (X = $[DIm]^+$, $[DImDm]^+$, and $[DPy]^+$) GDILs tends to be arranged in parallel to the GNF, and the other one is bent upward to the GNF. The vdW interactions between these dications and GNF are present via cooperative $\pi\cdots\pi$ and C−H$\cdots\pi$ interactions. For the $[X][BF_4]$, $[X][PF_6]$, and $[X][Tf_2N]$ (X = $[DAm]^+$ and $[DPyrr]^+$) GDILs, the $[DPyrr]^+$ non-aromatic dication and $[DAm]^+$ aliphatic-tetraalkylammonium dication are adsorbed on the GNF through C−H$\cdots\pi$ interactions. From these results, it is concluded that the vdW interactions are responsible for the adsorption of GDILs on GNF. ChelpG charge analysis at the M06-2X/cc-pVDZ level of theory indicates that the overall charge on the dications, anions, and GNF changes with the adsorption of GDILs on the GNF. The results of ChelpG charge analysis for the GDIL@GNF complexes are summarized in Table 2.

According to Table 2, the amount of charge transfer between GDILs and GNF ($\Delta Q_{\text{charge on GNF}}$) is calculated by calculation of the residual charge on the GNF in the GDIL@GNF complexes. The negative values of $\Delta Q_{\text{charge on GNF}}$ show that the charge transfer occurs from GDILs to GNF, whereas the positive values show the opposite direction. The amount of $\Delta Q_{\text{charge on GNF}}$ and the direction of charge transfer between GDILs and the GNF are generally different. For example, the adsorption of $[DAm][PF_6]$ on the GNF induces a charge of −0.0878e on the GNF surface, whereas the adsorption of $[DImDm][Tf_2N]$ induces a charge of 0.0589e on the surface. Furthermore, our results indicate that the charge transfer in the complexes is not considerable, which can be due to weak vdW adsorption of GDILs on the GNF. The adsorption of GDILs on the GNF changes the charge on the dications and anions in the complexes. The change in charge on the dications (ΔQ_{cation}) and anions (Δq_{anion}) was calculated and is listed in Table 2. For example, with the adsorption of $[DAm][BF_4]$ GDIL on the GNF surface, the $[DAm]^+$ cation becomes less positive by 0.1707e and the $[BF_4]^-$ anion becomes less negative by 0.1851e. This induces a charge of −0.0144e on the GNF surface.

The calculated adsorption energy (E_{ads}) values for all the GDIL@GNF complexes are summarized in Table 2 and compared in Figure 3. The negative E_{ads} values recommend that the formation of GDIL@GNF complexes is possible from the energetic point of view. The E_{ads} values for these complexes are in the range of −16.91 to −29.29 kcal/mol. According to the E_{ads} results, the highest E_{ads} values for interaction of GDILs containing $[BF_4]^-$, $[PF_6]^-$, and $[Tf_2N]^-$ anions with the GNF are observed for the $[DPy][BF_4]$@GNF (−23.56 kcal/mol), $[DPy][PF_6]$@GNF (−29.29 kcal/mol), and $[DPyrr][Tf_2N]$@GNF (−24.74 kcal/mol) complexes, respectively. In addition to E_{ads} values, other thermodynamic properties such as $\Delta S_{\text{GDIL@GNF}}$, $\Delta H_{\text{GDIL@GNF}}$, and $\Delta G_{\text{GDIL@GNF}}$ were calculated for adsorption of GDILs on the GNF, summarized in Table 2 and compared in Figure 3. The adsorption of GDILs on the GNF decreases the degrees of freedom of the GDILs and leads to the observation of negative $\Delta S_{\text{GDIL@GNF}}$ values for the formation of the GDIL@GNF complexes. Nevertheless, the $\Delta H_{\text{GDIL@GNF}}$ term controls the interaction, ensuring that the GDIL@GNF formation is a favorable process. Furthermore, all calculated $\Delta G_{\text{GDIL@GNF}}$ values are negative and show that the GDIL@GNF formation is exothermic. According to the

https://doi.org/10.1021/acsomega.3c06581
ACS Omega 2024, 9, 7575−7587

Table 2. Adsorption Energy (E_{ads} in kcal/mol), Change in Enthalpy ($\Delta H_{GDIL@GNF}$ in kcal/mol), Change in Entropy ($\Delta S_{GDIL@GNF}$ in cal/mol·K), Change in Gibbs Free Energy ($\Delta G_{GDIL@GNF}$ in kcal/mol), the Difference in the Sum of Electron Density ($\Delta\sum\rho(r)$ in a.u.), Charge Changes on the Dications (ΔQ_{cation} in e), Charge Changes on the Anions (Δq_{anion} in e), and the Amount of Charge Transfer between GDILs and GNF ($\Delta Q_{charge\ on\ GNF}$ in e) Calculated at the M06-2X/cc-pVDZ Level of Theory

structure	E_{ads}	$\Delta H_{GDIL@GNF}$	$\Delta S_{GDIL@GNF}$	$\Delta G_{GDIL@GNF}$	[a] $\Delta\sum\rho(r)$	[b,e] Δq_{cation}	[c,e] Δq_{anion}	[d] $\Delta Q_{charge\ on\ GNF}$
[DAm][BF_4]@GNF	−19.85	−19.39	−46.28	−5.59	0.1438	0.1707	−0.1851	−0.0144
[DAm][PF_6]@GNF	−18.96	−20.03	−42.81	−7.27	0.0475	0.3141	−0.4019	−0.0878
[DAm][Tf_2N]@GNF	−21.98	−21.97	−51.73	−6.54	0.0282	0.3399	−0.3657	−0.0258
[DIm][BF_4]@GNF	−16.91	−14.63	−40.88	−2.44	0.1749	0.0158	0.0287	0.0445
[DIm][PF_6]@GNF	−18.37	−16.97	−38.44	−5.51	0.0385	0.1344	−0.1065	0.0279
[DIm][Tf_2N]@GNF	−19.12	−18.43	−49.12	−3.78	0.0628	−0.0334	0.0554	0.0220
[DImDm][BF_4]@GNF	−18.94	−17.59	−37.99	−6.26	0.0177	−0.0299	0.0560	0.0261
[DImDm][PF_6]@GNF	−19.71	−18.85	−38.17	−7.47	0.0016	0.0699	−0.0722	−0.0023
[DImDm] [Tf_2N]@GNF	−18.67	−15.65	−48.76	−1.12	0.0210	0.3933	−0.3344	0.0589
[DPy][BF_4]@GNF	−23.56	−26.85	−53.15	−11.00	0.0448	0.2726	−0.3049	−0.0323
[DPy][PF_6]@GNF	−29.29	−33.72	−52.19	−18.16	0.0534	0.2793	−0.2795	−0.0002
[DPy][Tf_2N]@GNF	−19.81	−22.70	−54.76	−6.37	0.0229	−0.1401	0.1117	−0.0284
[DPyrr][BF_4]@GNF	−18.99	−16.58	−36.83	−5.60	0.0010	0.1715	−0.1171	0.0544
[DPyrr][PF_6]@GNF	−21.21	−23.44	−47.48	−9.28	0.0660	0.3590	−0.3683	−0.0093
[DPyrr][Tf2N]@GNF	−24.74	−26.79	−52.38	−11.17	0.0263	0.1920	−0.1984	−0.0064

[a] $\Delta\sum\rho(r)$ is the difference of the sum of electron density ($\sum\rho(r)$) values at the bond critical points (BCPs) formed between the dications and anions in the GDILs before and after adsorption on the GNF. [b] $\Delta q_{(cation)} = q_{cation\ in\ GDIL(before\ adsorption)} - q_{cation\ in\ GDIL(after\ adsorption)}$. [c] $\Delta q_{(anion)} = q_{anion\ in\ GDIL(before\ adsorption)} - q_{anion\ in\ GDIL(after\ adsorption)}$. [d] Charge of GNF before adsorption is zero. [e] The positive and negative sign of Δq for dications and anions ($\Delta q_{(cation)}$ and $\Delta q_{(anion)}$) means that the charge is gained and lost by the components after adsorption of GDILs on the GNF, respectively.

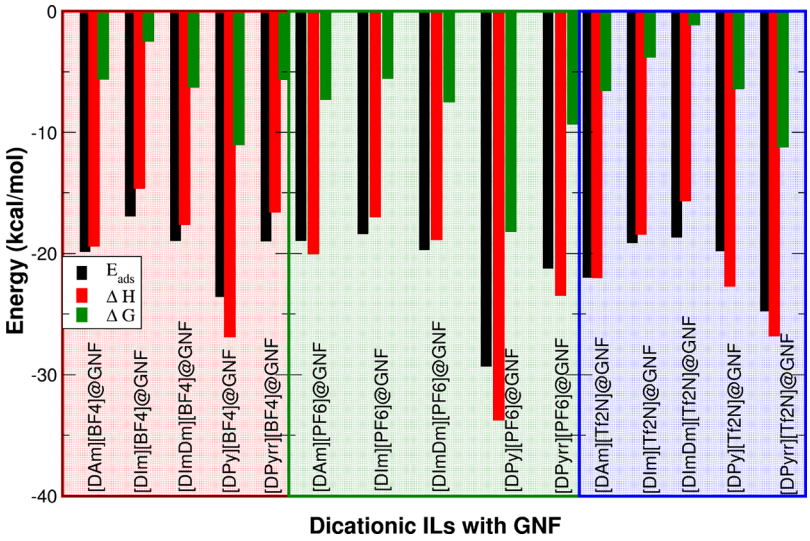

Figure 3. Comparison of adsorption energy (E_{ads}), enthalpy change ($\Delta H_{GDIL@GNF}$), and Gibbs free energy change ($\Delta G_{GDIL@GNF}$) of the GDIL@GNF complexes.

$\Delta G_{GDIL@GNF}$ results, the highest $\Delta G_{GDIL@GNF}$ values for interaction of GDILs containing $[BF_4]^-$, $[PF_6]^-$, and $[Tf_2N]^-$ anions with the GNF are observed for the [DPy][BF_4]@GNF (−11.0 kcal/mol), [DPy][PF_6]@GNF (−18.16 kcal/mol), and [DPyrr][Tf_2N]@GNF (−11.17 kcal/mol) complexes, respectively, following the result observed for the E_{ads} values.

We also investigated the effect of GDIL adsorption on the reactivity parameters of GNF, including the HOMO−LUMO energy gap (E_g), chemical potential (μ), chemical hardness (η), and electrophilicity index (ω), by calculating the HOMO and LUMO orbital energies. These parameters were calculated at the M06-2X/cc-pVDZ level of theory and are listed in Table S1.

From the results, we found that the μ value of GNF, as a measure of electronegativity property, decreases upon adsorption of GDILs. The resistance of a molecule against the change of its electron cloud and chemical stability is understood by calculating the chemical hardness (η) value. The η term is associated with the energy difference between the HOMO and LUMO orbitals, known as E_g. The larger the E_g value is, the harder is the molecule, and the higher is the stability of the molecule. As shown in Table S1, the E_g and η values for the GNF are 4.32 and 2.16 eV, respectively. These values for the GNF decrease upon the adsorption of GDILs. The most significant change in E_g and η values of GNF is observed upon the adsorption of [DPy][BF_4] GDIL (E_g = 3.95 eV and η = 1.97 eV). Furthermore, the electrophilicity index

https://doi.org/10.1021/acsomega.3c06581
ACS Omega 2024, 9, 7575−7587

(ω) values, as a measure of the electrophilic nature of a molecule, were calculated for the GNF and GDIL@GNF complexes. Our findings show that the adsorption of GDILs on the GNF leads to an increase in the electrophilic nature of GNF. As seen from Table S1, the greatest increase in the ω value is observed with the adsorption of [DPyrr][BF_4] GDIL on the GNF.

3.3. UV−Vis Absorption Spectra and TDM Heat Maps.

To understand the adsorption effect of GDILs on the optical properties of GNF surface, the time-dependent density functional theory (TDDFT) calculation was performed at the TD-M06-2X/cc-pVDZ level of theory. The calculated absorption spectra of GNF and its complexes with the GDILs are shown in Figure 4. These spectra are characterized by the

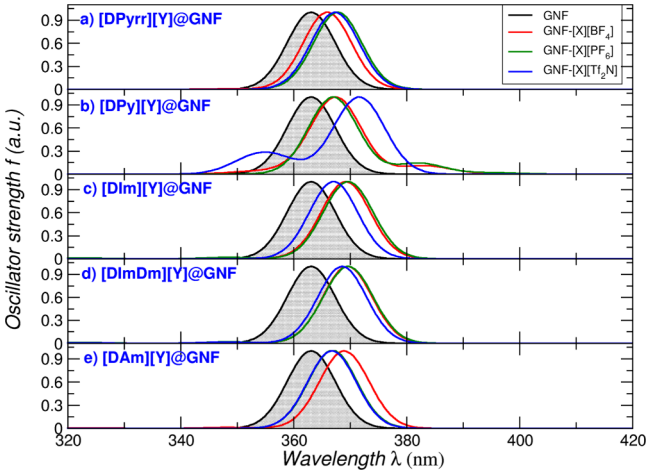

Figure 4. UV−vis absorption spectra of GNF and GDIL@GNF complexes were calculated at the TD-M06-2X/cc-pVDZ level of theory.

results listed in Table S2, including the excitation energy (E), excitation wavelength (λ), oscillator strength (f), excitation coefficients, main transitions, and excitation states (n).

As seen in Figure 4, the absorption spectrum of GNF yields a single peak at λ = 363 nm related to the $\pi_{(C=C)} \rightarrow \pi^*_{(C=C)}$ (HOMO−1 → LUMO+1) electronic transitions. Findings show that the adsorption of GDILs does not cause important changes in the shape of the GNF spectrum. The slight changes are only observed with adsorption of [DPy][Y] (Y = $[BF_4]^-$, $[PF_6]^-$, and $[Tf_2N]^-$) GDILs. The new low-intensity peaks at λ = 388 nm (HOMO → LUMO+2), λ = 382 nm (HOMO−1 → LUMO+3), and λ = 357 nm (HOMO → LUMO+3), respectively, observed in the absorption spectra of [DPy][BF_4]@GNF, [DPy][PF_6]@GNF, and [DPy][Tf_2N]@GNF complexes correspond to the $\pi_{(C=C)} \rightarrow \pi^*_{(C=C)}$ electronic transitions between the $[DPy]^+$ dication and GNF. Furthermore, a common feature in the spectra of the GDIL@GNF complexes is the redshift of the single peak in the GNF spectrum (λ = 363 nm) with the adsorption of GDILs.

To analyze and interpret the electronic excitation processes in the GDIL@GNF complexes, the transition density matrix (TDM) heat maps of the GDIL@GNF complexes are presented in Figure S6, and those of [DPy][Y]@GNF ([Y] = $[BF_4]^-$, $[PF_6]^-$, and $[Tf_2N]^-$) complexes are shown in Figure 5. In addition, the charges transferred between the GNF and constituents of the GDILs ([dication] and [anion]) for each excitation state are listed in Table S3.

The TDM heat maps are defined by the self-defined fragments and are inferred by a self-defined fragment index of electron transfer. As seen from the figures, the TDM heat maps of GDIL@GNF complexes are defined based on three fragments including fragment 1 (GNF), fragment 2 ([dication]$^+$ = $[DAm]^+$, $[DIm]^+$, $[DImDm]^+$, $[DPy]^+$, and $[DPyrr]^+$), and fragment 3 ([anion]$^-$ = $[BF_4]^-$, $[PF_6]^-$, and $[Tf_2N]^-$). In the TDM heat maps, the y axis refers to the originating fragment (corresponding to electron position), and the x axis refers to the receiving fragment (corresponding to hole position) for the excited electron. Furthermore, the diagonal and off-diagonal elements in the TDM heat maps show the intra- and interfragment electron transfer related to the excitation states in the complexes. As seen from the TDM heat maps, the values of diagonal elements in the [X][Y]@GNF ([X] = $[DAm]^+$, $[DIm]^+$, $[DImDm]^+$, and $[DPyrr]^+$); [Y] = $[BF_4]^-$, $[PF_6]^-$, and $[Tf_2N]^-$) complexes are more important than those of off-diagonal elements. This result reveals that the nature of electron excitation in the complexes is intrafragment electron transfer and is associated with the $\pi_{(C=C)} \rightarrow \pi^*_{(C=C)}$ electronic transitions in the GNF.

As seen in Figure 5, the electron transfer for the excitation states in the [DPy][Y]@GNF ([Y] = $[BF_4]^-$, $[PF_6]^-$, and $[Tf_2N]^-$) complexes is different from other complexes. In these complexes, both inter- and intrafragment electron transfers are observed. For the [DPy][BF_4]@GNF complex, two excitation states of S0 → S3 and S0 → S5 are observed in the TDM heat maps. The electron transfer related to the S0 → S3 excitation state occurs simultaneously through intrafragment electron transfer in the GNF (the yellow color) and interfragment electron transfer from $[DPy]^+$ to GNF (the red color), leading to a charge transfer of about 0.89313e between the GNF and $[DPy]^+$. For the S0 → S5, the electron transfer occurs mainly within the GNF (the red color). For the [DPy][PF_6]@GNF complex, two excitation states including S0 → S6 and S0 → S7 are observed in the TDM heat maps. According to the colors in the TDM heat map of S0 → S6, the hole is distributed on the GNF, and the electrons appear mainly on $[DPy]^+$ and to some extent on GNF. This shows that the electron transfer happens mainly from the $[DPy]^+$ to GNF (the red color) and partially within the GNF (cyan color), leading to a charge transfer of about 0.76550 between the GNF and $[DPy]^+$. Since off-diagonal elements in the TDM heat map of S0 → S7 are not quite large, electron excitation doesn't make a noteworthy electron transfer between various fragments and happens through the electron and hole distributed on the GNF (the red color). In the case of [DPy][Tf_2N]@GNF complex, the S0 → S3 and S0 → S7 excitation states occur through the electrons that appeared on the GNF and $[DPy]^+$ fragments and the hole distributed on the GNF surface. According to the colors, we find that electron transfer for the S0 → S3 occurs mainly within the GNF fragment and to some extent from $[DPy]^+$ to GNF. For the S0 → S7 excitation state, this behavior is reversed, and the electron transfer occurs mainly from $[DPy]^+$ fragment to the GNF and some extent within the GNF. In addition, the S0 → S3 and S0 → S7 excitation states lead to the charge transfer of about 0.33835e and 0.68509e between the GNF and $[DPy]^+$, respectively.

4. CONCLUSIONS

In this study, the physisorption between GDILs and GNF surface has been investigated by employing the M06-2X-D3/

https://doi.org/10.1021/acsomega.3c06581
ACS Omega 2024, 9, 7575−7587

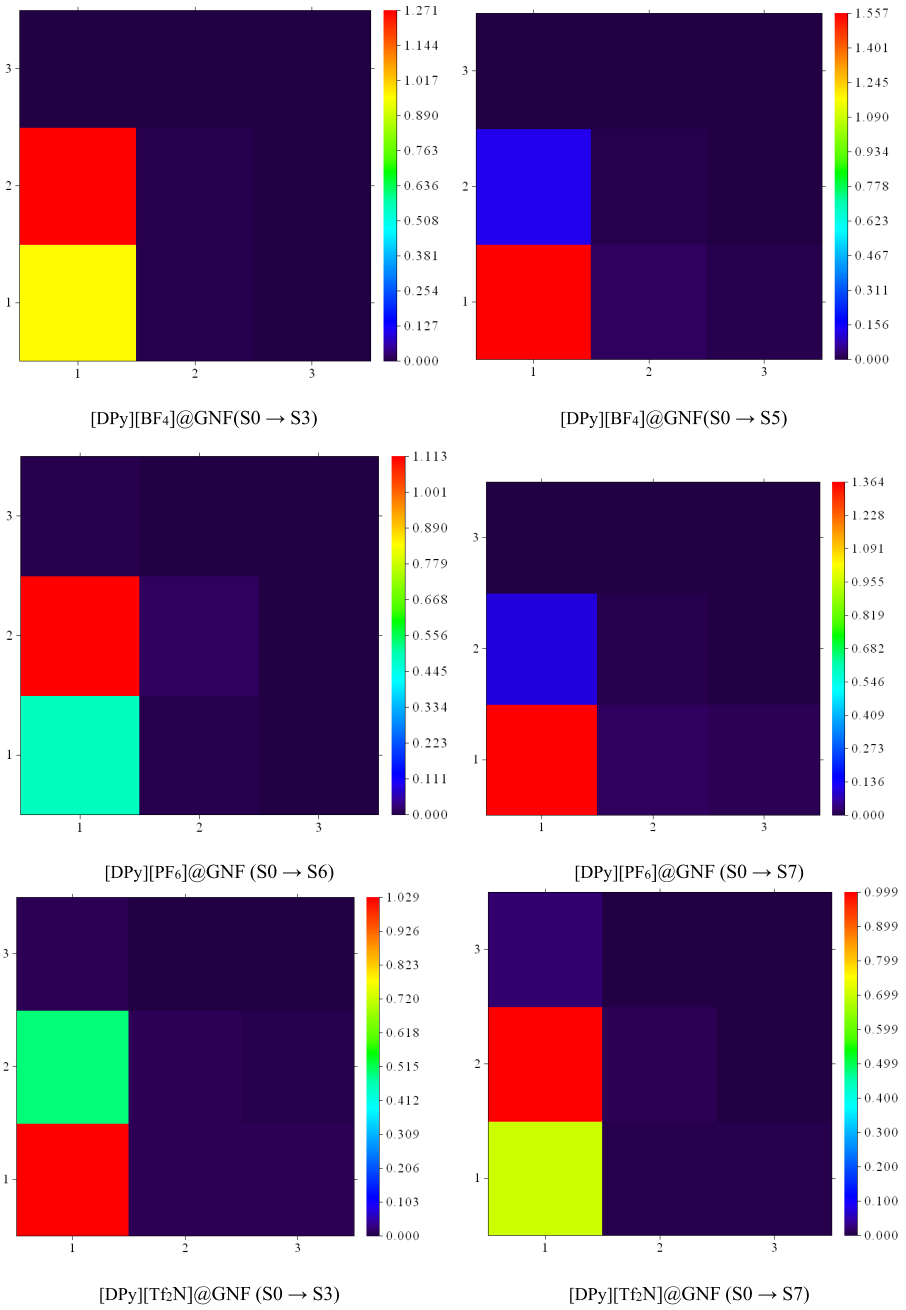

Figure 5. TDM heat maps of the [DPy][Y]@GNF ([Y] = $[BF_4]^-$, $[PF_6]^-$, and $[Tf_2N]^-$) complexes. In these maps, 1, 2, and 3 terms are the GNF, $[DPy]^+$, and $[Y]^-$, respectively. The *x* and *y* axes are the receiving and originating fragments for the excited electron, respectively.

cc-pVDZ level of theory. Our calculations show that the anions in the structure of GDILs are stabilized near the dications through electrostatic interactions, hydrogen bonding (H-bonding) interactions, and van der Waals (vdW) interactions, including C−H···F, C−H···O═S, C−H···N, and π···X (X = N, O, F). The calculation of binding energy (E_b) values shows that the stability of GDILs follows the order [X][BF_4] > [X][Tf_2N] > [X][PF_6] (X = $[DAm]^+$, $[DIm]^+$, $[DImDm]^+$, $[DPy]^+$, and $[DPyrr]^+$). Findings show that the adsorption of GDILs on the GNF is favorable and happens through weak vdW interactions, leading to a decrease in the strength of intermolecular interactions between the dications and anions in the GDILs. Furthermore, the calculation of reactivity parameters shows that the μ, η, and E_g values of GNF decrease upon the adsorption of GDILs, whereas the ω values increase. Our results indicate that the highest E_{ads} values for adsorption of GDILs containing $[BF_4]^-$, $[PF_6]^-$, and $[Tf_2N]^-$ anions on the GNF are observed for the [DPy][BF_4]@GNF (−23.56 kcal/mol), [DPy][PF_6]@GNF (−29.29 kcal/mol), and [DPyrr][Tf_2N]@GNF (−24.74 kcal/mol) complexes, respectively.

The UV−vis results show that the absorption peak in the GNF spectrum (at λ = 363 nm) is red-shifted upon the adsorption of GDILs. Also, it is worth mentioning that the adsorption of GDILs does not cause important changes in the shape of the GNF spectrum, and only a new peak appears upon the adsorption of [DPy][Y] (Y = $[BF_4]^-$, $[PF_6]^-$, and $[Tf_2N]^-$), corresponding to the $\pi_{(C=C)} \rightarrow \pi^*_{(C=C)}$ electronic transitions between the $[DPy]^+$ dication and GNF. The TDM heat maps revealed that the nature of electron excitation in the

https://doi.org/10.1021/acsomega.3c06581
ACS Omega 2024, 9, 7575−7587

[X][Y]@GNF ([X] = $[DAm]^+$, $[DIm]^+$, $[DImDm]^+$, and $[DPyrr]^+$); [Y] = $[BF_4]^-$, $[PF_6]^-$, and $[Tf_2N]^-$) complexes is intrafragment electron transfer, corresponding to the $\pi_{(C=C)} \rightarrow \pi^*_{(C=C)}$ electronic transitions in the GNF. For the [DPy][Y]@GNF ([Y] = $[BF_4]^-$, $[PF_6]^-$, and $[Tf_2N]^-$) complexes, the intrafragment electron transfers in the GNF are accompanied by the interfragment electron transfers from $[DPy]^+$ to the GNF, which are responsible for the appearance of new peaks observed in the UV−vis absorption spectra of these complexes. By conducting these computational investigations, a better understanding is hoped to be gained of the chemical functionality of GDILs as suitable reaction media for stabilizing graphene sheets. This knowledge will contribute to the progress of efficient and environmentally sustainable methods for the dispersion and modification of graphene, which can have significant implications in various fields including coatings, sensing, electronics, energy management, photonics, and biomedical applications.

■ ASSOCIATED CONTENT

Supporting Information

The Supporting Information is available free of charge at https://pubs.acs.org/doi/10.1021/acsomega.3c06581.

Electrostatic potential (ESP) maps; noncovalent interaction (NCI) plots; AIM molecular graphs; reactivity parameters; UV−vis spectra data; transition density matrix (TDM) heat maps; and excited-states data (PDF)

■ AUTHOR INFORMATION

Corresponding Author

Mehdi Shakourian-Fard − *Department of Chemical Engineering, Birjand University of Technology, Birjand 97175/569, Iran;* orcid.org/0000-0002-5454-3698; Email: Shakourian@birjandut.ac.ir

Authors

Hamid Reza Ghenaatian − *Department of Physics, Jahrom University, Jahrom 74135-111, Iran*

Ganesh Kamath − *Dalzierfiver LLC, El Sobrante, California 94803, United States;* orcid.org/0000-0002-6957-1173

Complete contact information is available at: https://pubs.acs.org/10.1021/acsomega.3c06581

Author Contributions

Conceptualization: M.S.-F., G.K., H.R.G. Funding acquisition: M.S.-F., G.K., H.R.G. Investigation: M.S.-F., G.K., H.R.G. Methodology: all authors. Supervision: M.S.-F. Visualization: M.S.-F., G.K. Writing − original draft: M.S.-R., H.R.G. Writing − review and editing: all authors.

Notes

The authors declare no competing financial interest.

■ ACKNOWLEDGMENTS

We gratefully acknowledge the financial support from the Research Council of the Birjand University of Technology, and Jahrom University is gratefully acknowledged.

■ REFERENCES

(1) Rana, D. S.; Kalia, S.; Kumar, R.; Thakur, N.; Singh, R. K.; Singh, D. Two-dimensional layered reduced graphene oxide-tungsten disulphide nanocomposite for highly sensitive and selective determination of para nitrophenol. *Environ. Nanotechnol. Monit. Manag.* **2022**, *18*, No. 100724.

(2) Liu, Z.; He, T.; Jiang, Q.; Wang, W.; Tang, J. A review of heteroatomic doped two-dimensional materials as electrocatalysts for hydrogen evolution reaction. *Int. J. Hydrog. Energy* **2022**, *47* (69), 29698−29729.

(3) He, X.; Peng, H.; Xiong, Z.; Nie, X.; Wang, D.; Wang, G.; Liu, C. A sustainable and low-cost route to prepare magnetic particle-embedded ultra-thin carbon nanosheets with broadband microwave absorption from biowastes. *Carbon* **2022**, *198*, 195−206.

(4) Raza, S.; Ghasali, E.; Orooji, Y.; Lin, H.; Karaman, C.; Dragoi, E. N.; Erk, N. Two dimensional (2D) materials and biomaterials for water desalination; structure, properties, and recent advances. *Environ. Res.* **2023**, *219*, No. 114998.

(5) Li, T.; Shang, D.; Gao, S.; Wang, B.; Kong, H.; Yang, G.; Shu, W.; Xu, P.; Wei, G. Two-Dimensional Material-Based Electrochemical Sensors/Biosensors for Food Safety and Biomolecular Detection. *Biosensors* **2022**, *12*, 314.

(6) Fan, R.; Sun, L.; Shao, X.; Li, Y.; Zhao, M. Two-dimensional Dirac materials: Tight-binding lattice models and material candidates. *ChemPhysMater.* **2023**, *2* (1), 30−42.

(7) Reddy, Y. V. M.; Shin, J. H.; Palakollu, V. N.; Sravani, B.; Choi, C.-H.; Park, K.; Kim, S.-K.; Madhavi, G.; Park, J. P.; Shetti, N. P. Strategies, advances, and challenges associated with the use of graphene-based nanocomposites for electrochemical biosensors. *Adv. Colloid Interface Sci.* **2022**, *304*, No. 102664.

(8) Wang, G.-E.; Luo, S.; Di, T.; Fu, Z.; Xu, G. Layered Organic Metal Chalcogenides (OMCs): From Bulk to Two-Dimensional Materials. *Angew. Chem., Int. Ed.* **2022**, *61* (27), No. e202203151.

(9) VahidMohammadi, A.; Rosen, J.; Gogotsi, Y. The world of two-dimensional carbides and nitrides (MXenes). *Science* **2021**, *372*, No. eabf1581.

(10) Kausar, A.; Ahmad, I.; Zhao, T.; Eisa, M.; Aldaghri, O. Graphene Nanofoam Based Nanomaterials: Manufacturing and Technical Prospects. *Nanomanufacturing* **2023**, *3*, 37−56.

(11) Barai, D. P.; Bhanvase, B. A.; Sonawane, S. H. A Review on Graphene Derivatives-Based Nanofluids: Investigation on Properties and Heat Transfer Characteristics. *Ind. Eng. Chem. Res.* **2020**, *59* (22), 10231−10277.

(12) Cheng, Z.; Wang, R.; Wang, Y.; Cao, Y.; Shen, Y.; Huang, Y.; Chen, Y. Recent advances in graphene aerogels as absorption-dominated electromagnetic interference shielding materials. *Carbon* **2023**, *205*, 112−137.

(13) Mohan, V. B.; Lau, K.-t.; Hui, D.; Bhattacharyya, D. Graphene-based materials and their composites: A review on production, applications and product limitations. *Compos. B: Eng.* **2018**, *142*, 200−220.

(14) Mohammad, A.; Inamuddin, D. *Green solvents II: properties and applications of ionic liquids*; Springer, 2012.

(15) Guo, F.; Zhang, S.; Wang, J.; Teng, B.; Zhang, T.; Fan, M. Synthesis and Applications of Ionic Liquids in Clean Energy and Environment: A Review. *Curr. Org. Chem.* **2015**, *19* (5), 455−468.

(16) Javed, F.; Ullah, F.; Zakaria, M. R.; Akil, H. M. An approach to classification and hi-tech applications of room-temperature ionic liquids (RTILs): A review. *J. Mol. Liq.* **2018**, *271*, 403−420.

(17) Nie, L.; Cai, C.; Guo, R.; Yao, S.; Zhu, Z.; Hong, Y.; Guo, D. Ionic Liquid-Assisted DLLME and SPME for the Determination of Contaminants in Food Samples. *Separations* **2022**, *9*, 170.

(18) Trujillo-Rodríguez, M. J.; Nan, H.; Varona, M.; Emaus, M. N.; Souza, I. D.; Anderson, J. L. Advances of Ionic Liquids in Analytical Chemistry. *Anal. Chem.* **2019**, *91* (1), 505−531.

(19) Gan, C.; Liang, T.; Li, W.; Fan, X.; Li, X.; Li, D.; Zhu, M. Hydroxyl-terminated ionic liquids functionalized graphene oxide with good dispersion and lubrication function. *Tribol. Int.* **2020**, *148*, No. 106350.

(20) Fang, D.; Wen, J.; Yu, H.; Zhang, J.; You, X.; Liu, N. Ionic liquid functionalized polylactides: the effect of anions on catalytic activity and carbon nanotube dispersion. *Mater. Adv.* **2023**, *4* (3), 948−953.

(21) García, G.; Atilhan, M.; Aparicio, S. Theoretical Study on the Solvation of C60 Fullerene by Ionic Liquids. *J. Phys. Chem. B* **2014**, *118* (38), 11330−11340.
(22) García, G.; Atilhan, M.; Aparicio, S. Theoretical Study on the Solvation of C60 Fullerene by Ionic Liquids II: DFT Analysis of the Interaction Mechanism. *J. Phys. Chem. B* **2015**, *119* (33), 10616−10629.
(23) Bordes, E.; Morcos, B.; Bourgogne, D.; Andanson, J.-M.; Bussière, P.-O.; Santini, C. C.; Benayad, A.; Costa Gomes, M.; Pádua, A. A. H. Dispersion and Stabilization of Exfoliated Graphene in Ionic Liquids. *Front. Chem.* **2019**, 7223, DOI: 10.3389/fchem.2019.00223.
(24) Tunckol, M.; Durand, J.; Serp, P. Carbon nanomaterial−ionic liquid hybrids. *Carbon* **2012**, *50* (12), 4303−4334.
(25) Ciesielski, A.; Samorì, P. Supramolecular Approaches to Graphene: From Self-Assembly to Molecule-Assisted Liquid-Phase Exfoliation. *Adv. Mater.* **2016**, *28* (29), 6030−6051. (acccessed 2023/08/03).
(26) Quintas, P. Y.; Fiorentini, E. F.; Llaver, M.; González, R. E.; Wuilloud, R. G. State-of-the-art extraction and separation of enantiomers through the application of alternative solvents. *TrAC, Trends Anal. Chem.* **2022**, *157*, No. 116733.
(27) Cecchini, M. M.; Bendjeriou, A.; Mnasri, N.; Charnay, C.; Angelis, F. D.; Lamaty, F.; Martinez, J.; Colacino, E. Synthesis of novel multi-cationic PEG-based ionic liquids. *New J. Chem.* **2014**, *38* (12), 6133−6138.
(28) Cecchini, M. M.; Charnay, C.; De Angelis, F.; Lamaty, F.; Martinez, J.; Colacino, E. Poly(ethylene glycol)-Based Ionic Liquids: Properties and Uses as Alternative Solvents in Organic Synthesis and Catalysis. *ChemSusChem* **2014**, *7* (1), 45−65.
(29) Kaczmarek, D. K.; Czerniak, K.; Klejdysz, T. Dicationic ionic liquids as new feeding deterrents. *Chem. Pap.* **2018**, *72* (10), 2457−2466.
(30) Roohi, H.; Gildeh, S. F. G.; Ghauri, K.; Fathei, P. Physicochemical properties of the imidazolium-based dicationic ionic liquids (DILs) composed of ethylene π-spacer by changing the anions: a quantum chemical approach. *Ionics* **2020**, *26* (4), 1963−1988.
(31) Moosavi, M.; Khashei, F.; Sedghamiz, E. Molecular dynamics simulation of geminal dicationic ionic liquids [Cn(mim)2][NTf2]2 − structural and dynamical properties. *Phys. Chem. Chem. Phys.* **2018**, *20* (1), 435−448.
(32) Alavi, S. M.; Yeganegi, S. DFT study of structures and hydrogen bonds of imidazolium based halogen-free boron containing dicationic ionic liquids. *J. Mol. Liq.* **2018**, *256*, 330−343.
(33) Yeganegi, S.; Soltanabadi, A.; Farmanzadeh, D. Molecular Dynamic Simulation of Dicationic Ionic Liquids: Effects of Anions and Alkyl Chain Length on Liquid Structure and Diffusion. *J. Phys. Chem. B* **2012**, *116* (37), 11517−11526.
(34) Matsumoto, M.; Saito, Y.; Park, C.; Fukushima, T.; Aida, T. Ultrahigh-throughput exfoliation of graphite into pristine 'single-layer' graphene using microwaves and molecularly engineered ionic liquids. *Nat. Chem.* **2015**, *7* (9), 730−736.
(35) Li, S.; Feng, G.; Cummings, P. T. Interfaces of dicationic ionic liquids and graphene: a molecular dynamics simulation study. *J. Condens. Matter Phys.* **2014**, *26* (28), No. 284106.
(36) Kuhn, B. L.; Osmari, B. F.; Heinen, T. M.; Bonacorso, H. G.; Zanatta, N.; Nielsen, S. O.; Ranathunga, D. T. S.; Villetti, M. A.; Frizzo, C. P. Dicationic imidazolium-based dicarboxylate ionic liquids: Thermophysical properties and solubility. *J. Mol. Liq.* **2020**, *308*, No. 112983.
(37) Frizzo, C. P.; Bender, C. R.; Salbego, P. R. S.; Farias, C. A. A.; Villetti, M. A.; Martins, M. A. P. Heteroassembly Ability of Dicationic Ionic Liquids and Neutral Active Pharmaceutical Ingredients. *ACS Omega* **2018**, *3* (2), 2282−2291.
(38) Anderson, J. L.; Ding, R.; Ellern, A.; Armstrong, D. W. Structure and Properties of High Stability Geminal Dicationic Ionic Liquids. *J. Am. Chem. Soc.* **2005**, *127* (2), 593−604.
(39) Shakourian-Fard, M.; Jamshidi, Z.; Bayat, A.; Kamath, G. Meta-Hybrid Density Functional Theory Study of Adsorption of Imidazolium- and Ammonium-Based Ionic Liquids on Graphene Sheet. *J. Phys. Chem. C* **2015**, *119* (13), 7095−7108.
(40) Shakourian-Fard, M.; Kamath, G. The effect of defect types on the electronic and optical properties of graphene nanoflakes physisorbed by ionic liquids. *Phys. Chem. Chem. Phys.* **2017**, *19* (6), 4383−4395.
(41) Lynden-Bell, R. M.; Del Pópolo, M. G.; Youngs, T. G. A.; Kohanoff, J.; Hanke, C. G.; Harper, J. B.; Pinilla, C. C. Simulations of Ionic Liquids, Solutions, and Surfaces. *Acc. Chem. Res.* **2007**, *40* (11), 1138−1145.
(42) Ghatee, M. H.; Moosavi, F. Physisorption of Hydrophobic and Hydrophilic 1-Alkyl-3-methylimidazolium Ionic Liquids on the Graphenes. *J. Phys. Chem. C* **2011**, *115* (13), 5626−5636.
(43) Grimme, S. Accurate description of van der Waals complexes by density functional theory including empirical corrections. *J. Comput. Chem.* **2004**, *25* (12), 1463−1473. (acccessed 2023/08/03).
(44) Grimme, S. Semiempirical GGA-type density functional constructed with a long-range dispersion correction. *J. Comput. Chem.* **2006**, *27* (15), 1787−1799. (acccessed 2023/08/03).
(45) Grimme, S.; Antony, J.; Ehrlich, S.; Krieg, H. A consistent and accurate ab initio parametrization of density functional dispersion correction (DFT-D) for the 94 elements H-Pu. *J. Chem. Phys.* **2010**, *132* (15), No. 154104. From NLM.
(46) Mardirossian, N.; Head-Gordon, M. Thirty years of density functional theory in computational chemistry: An overview and extensive assessment of 200 density functionals. *Mol. Phys.* **2017**, *115*, 2315−58.
(47) Ruzanov, A.; Lembinen, M.; Ers, H.; García de la Vega, J. M.; Lage-Estebanez, I.; Lust, E.; Ivaništšev, V. B. Density Functional Theory Study of Ionic Liquid Adsorption on Circumcoronene Shaped Graphene. *J. Phys. Chem. C* **2018**, *122* (5), 2624−2631.
(48) Shakourian-Fard, M.; Ghenaatian, H. R.; Kamath, G.; Taimoory, S. M. Unraveling the effect of nitrogen doping on graphene nanoflakes and the adsorption properties of ionic liquids: A DFT study. *J. Mol. Liq.* **2020**, *312*, No. 113400.
(49) Shakourian-Fard, M.; Maryamdokht Taimoory, S.; Semeniuchenko, V.; Kamath, G.; Trant, J. F. The effect of ionic liquid adsorption on the electronic and optical properties of fluorographene nanosheets. *J. Mol. Liq.* **2018**, *268*, 206−214.
(50) Shakourian-Fard, M.; Kamath, G.; Jamshidi, Z. Trends in Physisorption of Ionic Liquids on Boron-Nitride Sheets. *J. Phys. Chem. C* **2014**, *118* (45), 26003−26016.
(51) Torkzadeh, M.; Moosavi, M. A combined molecular dynamics simulation and quantum mechanics study on the physisorption of biodegradable CBNAILs on h-BN nanosheets. *Chem. Phys.* **2018**, *149* (7). DOI: 10.1063/1.5039476. (acccessed 12/14/2023).
(52) Talaei, R.; Khalili, B.; Mokhtary, M. Modulation of opto-electronic properties of the functionalized hexagonal boron nitride nanosheets with tunable aryl alkyl ionic liquids (TAAILs): Defect based analysis. *J. Mol. Liq.* **2020**, *304*, No. 112696.
(53) Shakourian-Fard, M.; Bayat, A.; Kamath, G. Effect of mono-vacant defects on the opto-electronic properties of ionic liquid functionalized hexagonal boron-nitride nanosheets. *J. Mol. Liq.* **2018**, *249*, 1172−1182.
(54) Roohi, H.; Ghauri, K.; Salehi, R. Non-covalent green functionalization of boron nitride nanotubes with tunable aryl alkyl ionic liquids: A quantum chemical approach. *J. Mol. Liq.* **2017**, *243*, 22−40.
(55) Frisch, M. J. *Gaussian09*. http://www.gaussian.com/ 2009.
(56) Boys, S. F.; Bernardi, F. The calculation of small molecular interactions by the differences of separate total energies. Some procedures with reduced errors. *Mol. Phys.* **1970**, *19* (4), 553−566.
(57) Lowdin, P.-O. *Advances in quantum chemistry*; Academic Press, 1979.
(58) Miertuš, S.; Scrocco, E.; Tomasi, J. Electrostatic interaction of a solute with a continuum. A direct utilizaion of AB initio molecular potentials for the prevision of solvent effects. *Chem. Phys.* **1981**, *55* (1), 117−129.

https://doi.org/10.1021/acsomega.3c06581
ACS Omega 2024, 9, 7575−7587

(59) Breneman, C. M.; Wiberg, K. B. Determining atom-centered monopoles from molecular electrostatic potentials. The need for high sampling density in formamide conformational analysis. *J. Comput. Chem.* **1990**, *11* (3), 361−373. (acccessed 2023/08/03).
(60) Geerlings, P.; De Proft, F.; Langenaeker, W. Conceptual Density Functional Theory. *Chem. Rev.* **2003**, *103* (5), 1793−1874.
(61) Roy, R. K.; Saha, S. Studies of regioselectivity of large molecular systems using DFT based reactivity descriptors. *Annu. Rep. Prog. Chem., Sect. C: Phys. Chem.* **2010**, *106* (0), 118−162. DOI: 10.1039/B811052M.
(62) Parr, R. G.; Pearson, R. G. Absolute hardness: companion parameter to absolute electronegativity. *J. Am. Chem. Soc.* **1983**, *105* (26), 7512−7516.
(63) Koopmans, T. Über die Zuordnung von Wellenfunktionen und Eigenwerten zu den Einzelnen Elektronen Eines Atoms. *Physica* **1934**, *1* (1), 104−113.
(64) Cioslowski, J. A Theory of Molecules: Atoms In *Molecules. A Quantum Theory*. Richard, FW Bader. Clarendon (Oxford University Press): New York, 1990. xviii, 438 pp. Cioslowski, J.A Theory of Molecules: Atoms In Molecules. A Quantum Theory. Richard FW Bader. Clarendon (Oxford University Press), New York, 1990. xviii, 438 pp., illus. $120. International Series of Monographs on Chemistry, 22*Science* **1991**, *252* (5012), 1566−1567.
(65) Schönbohm. Imnovative software. *J. Comput. Chem.* **2001**, *22*, 545.
(66) Lu, T.; Chen, F. Multiwfn: A multifunctional wavefunction analyzer. *J. Comput. Chem.* **2012**, *33* (5), 580−592. (acccessed 2023/08/03).
(67) Humphrey, W.; Dalke, A.; Schulten, K. VMD: Visual molecular dynamics. *J. Mol. Graph.* **1996**, *14* (1), 33−38.
(68) Johnson, E. R.; Keinan, S.; Mori-Sánchez, P.; Contreras-García, J.; Cohen, A. J.; Yang, W. Revealing Noncovalent Interactions. *J. Am. Chem. Soc.* **2010**, *132* (18), 6498−6506.
(69) Shirota, H.; Mandai, T.; Fukazawa, H.; Kato, T. Comparison between Dicationic and Monocationic Ionic Liquids: Liquid Density, Thermal Properties, Surface Tension, and Shear Viscosity. *J. Chem. Eng. Data* **2011**, *56* (5), 2453−2459.

https://doi.org/10.1021/acsomega.3c06581
ACS Omega 2024, 9, 7575−7587